

Electronic Supplementary Information

Mass Transport-Enhanced Electrodeposition of Ni-S-P-O Films on Nickel Foam for Electrochemical Water Splitting

Raul A. Marquez-Montes[†], Kenta Kawashima[†], Yoon Jun Son^{††}, Jason A. Weeks[†], Ho-Hyun Sun^{††}, Hugo Celio[‡], Víctor H. Ramos-Sánchez^{‡‡} and C. Buddie Mullins^{†,††,‡,§,§§,}*

[†] Department of Chemistry, The University of Texas at Austin, Austin, Texas 78712, United States.

^{††} McKetta Department of Chemical Engineering, The University of Texas at Austin, Austin, Texas 78712, United States.

[‡] Texas Materials Institute, The University of Texas at Austin, Texas 78712, United States.

^{‡‡} Facultad de Ciencias Químicas, Universidad Autónoma de Chihuahua, Chihuahua, Chihuahua 31125, México.

[§] Center for Electrochemistry, The University of Texas at Austin, Austin, Texas 78712, United States.

^{§§} H2@UT, The University of Texas at Austin, Texas 78712, United States.

* Corresponding author: mullins@che.utexas.edu

Number of pages: 35

Number of figures: 26

Number of tables: 6

Detailed Experimental Methods

Cleaning of NF substrates

NF pieces ($40 \times 30 \times 1.6$ mm) were cleaned in 50 mL of the following solutions while in an ultrasonic bath for 15 min each: (1) acetone, (2) ethanol, (3) 3 M HCl, and (4) deionized water.

Calculation of faradaic efficiencies (FEs)

For oxygen production, FEs were estimated as depicted in Equation S1:

$$FE = \frac{n_{O_2} \cdot z \cdot F \cdot (1000)}{j \cdot A \cdot t} \quad (S1)$$

where n_{O_2} represents the number of moles of O_2 generated every 2 h (according to water displacement in a 50 mL burette every 2 h), F is Faraday's constant ($96485.3 \text{ C} \cdot \text{mol}^{-1}$), z is the number of electrons transferred (4 for O_2), j is the applied current density ($10 \text{ mA} \cdot \text{cm}^{-2}$), A is the geometric electrode area (12 cm^2) and t the time in seconds (7200 seconds). For hydrogen production, FEs were estimated as follows:

$$FE = \frac{n_{H_2} \cdot z \cdot F \cdot (1000)}{j \cdot A \cdot t} \quad (S2)$$

where n_{H_2} is the number of moles of H_2 . In this case, z equals 2 for H_2 production, and t was always equal to 7200 seconds.

Electrodeposition in a conventional electrochemical cell

The electrodes were fixed at a constant separation (1 cm) using alligator clips and introduced vertically in a 250 mL beaker with ~200 mL of plating bath. The solution was mixed with a magnetic stir bar (1 cm) at 1200 rpm. The beaker was placed on top of a hotplate at 25°C .

Supplementary Tables and Figures

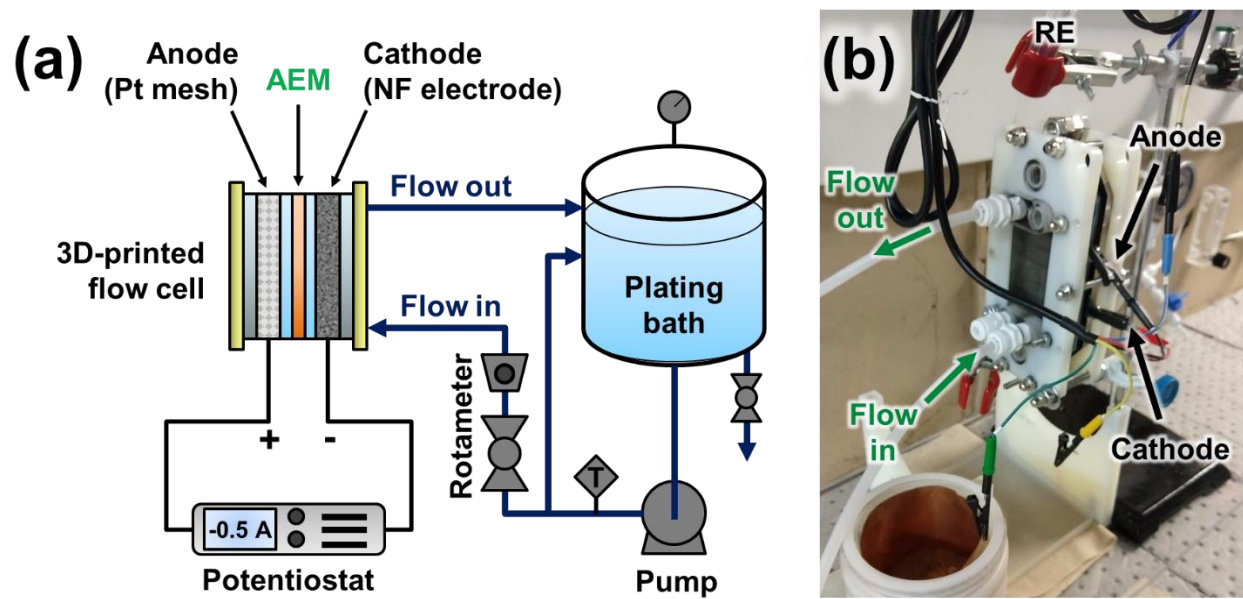


Figure S1. Flow cell experimental configuration: (a) flow scheme and electrodeposition configuration and (b) photo of the assembled electrochemical flow cell.

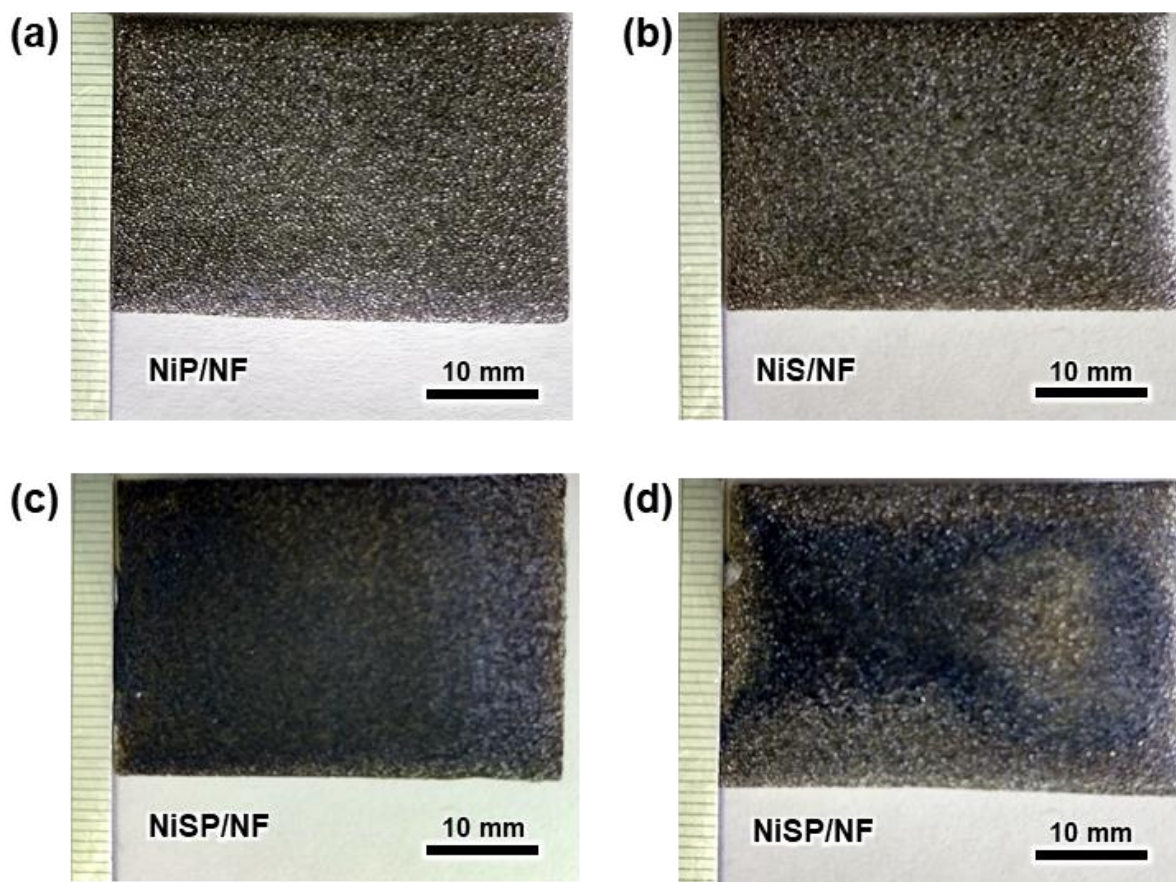


Figure S2. Digital photos of the as-prepared NF electrodes obtained under continuous forced flow ($6 \text{ L} \cdot \text{h}^{-1}$) in the flow cell: (a) NiP/NF, (b) NiS/NF and (c) NiSP/NF; (d) NiSP/NF electrode prepared with magnetic stirring (1200 rpm) in a conventional electrochemical cell. Conditions: electrodeposition during 30 min at $-50 \text{ mA} \cdot \text{cm}^{-2}$.

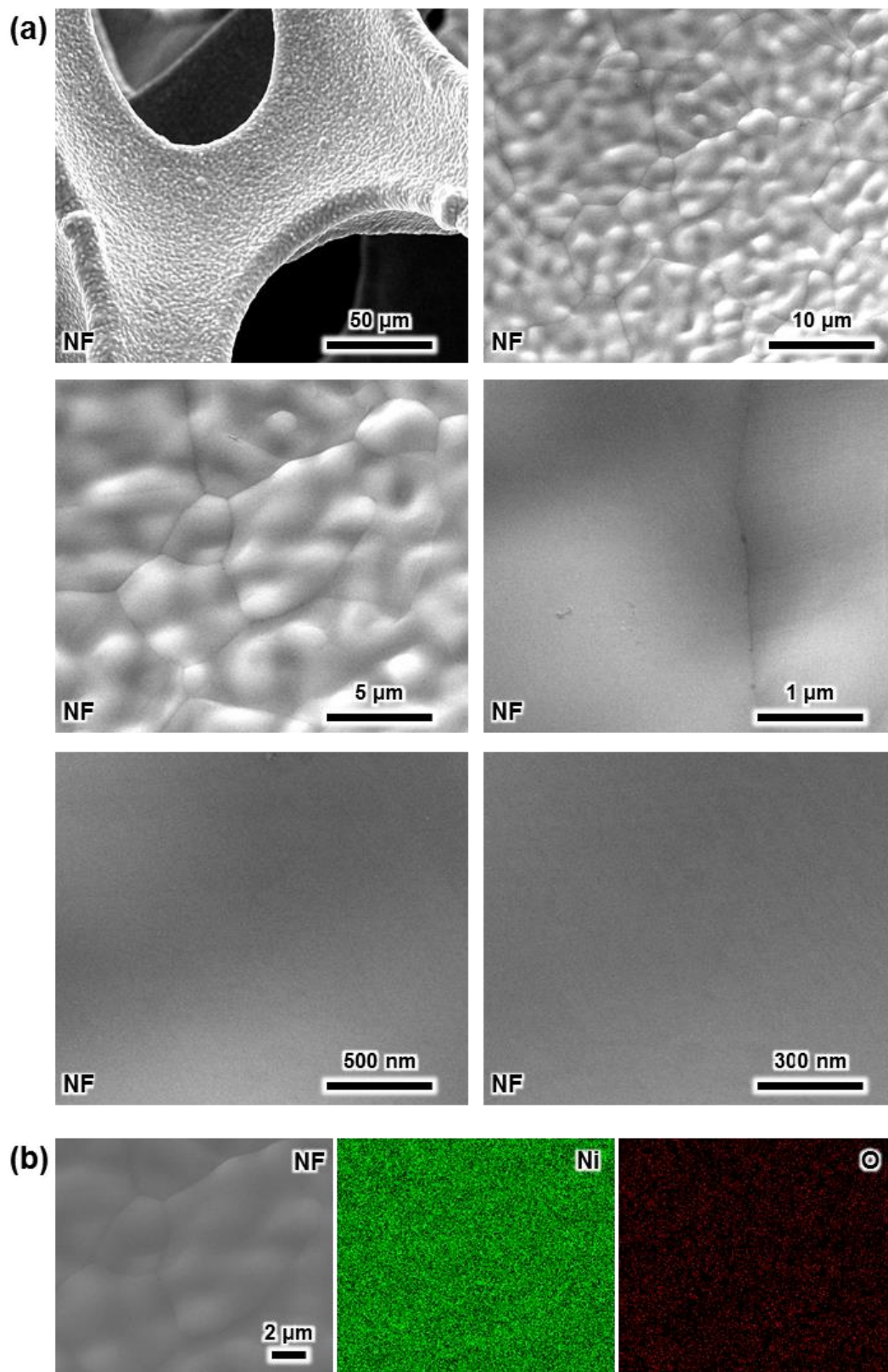


Figure S3. Physicochemical characterization of pristine nickel foam sample: (a) SEM images at different magnifications and (b) elemental mappings.

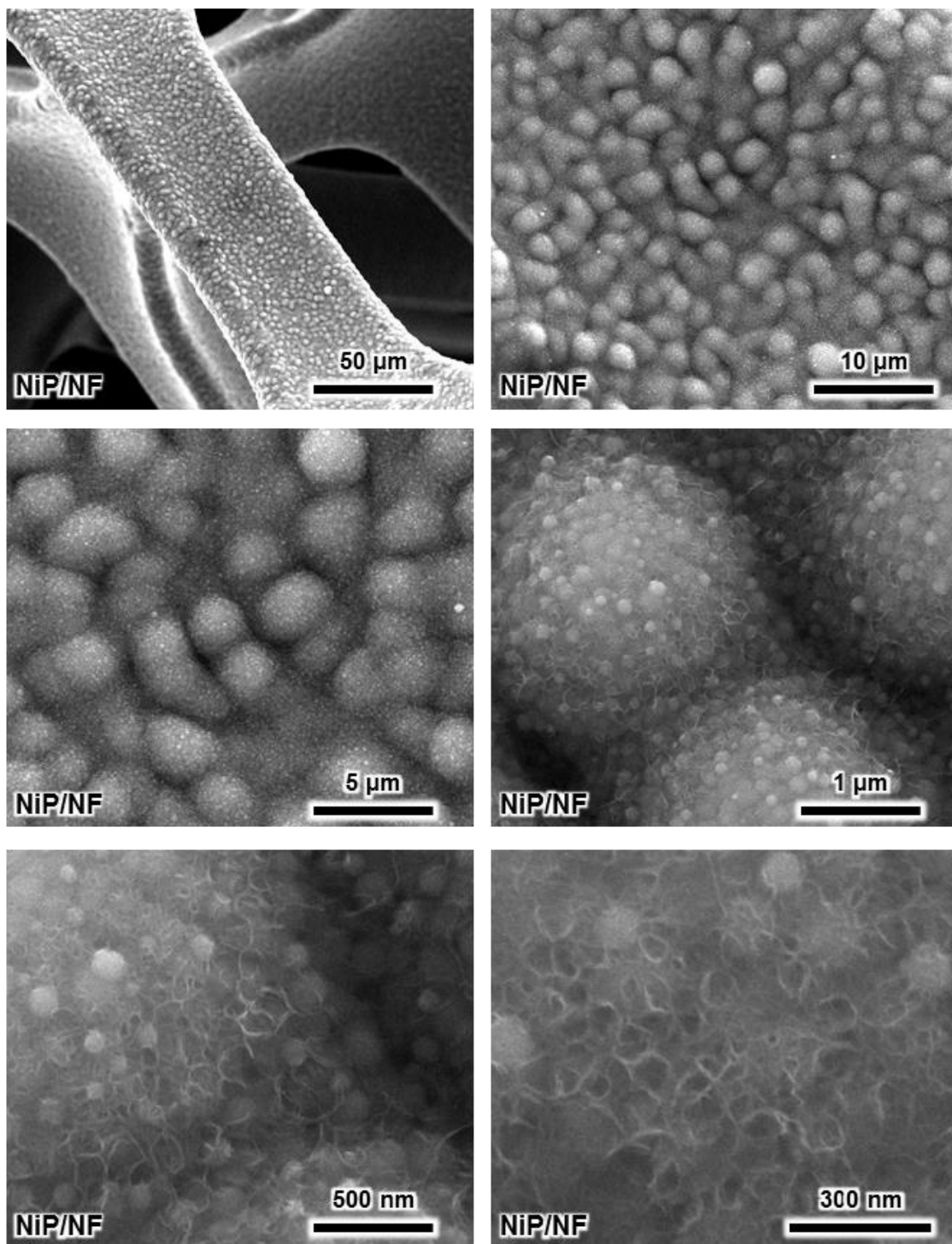


Figure S4. SEM images of the pristine NiP/NF electrode at different magnifications.

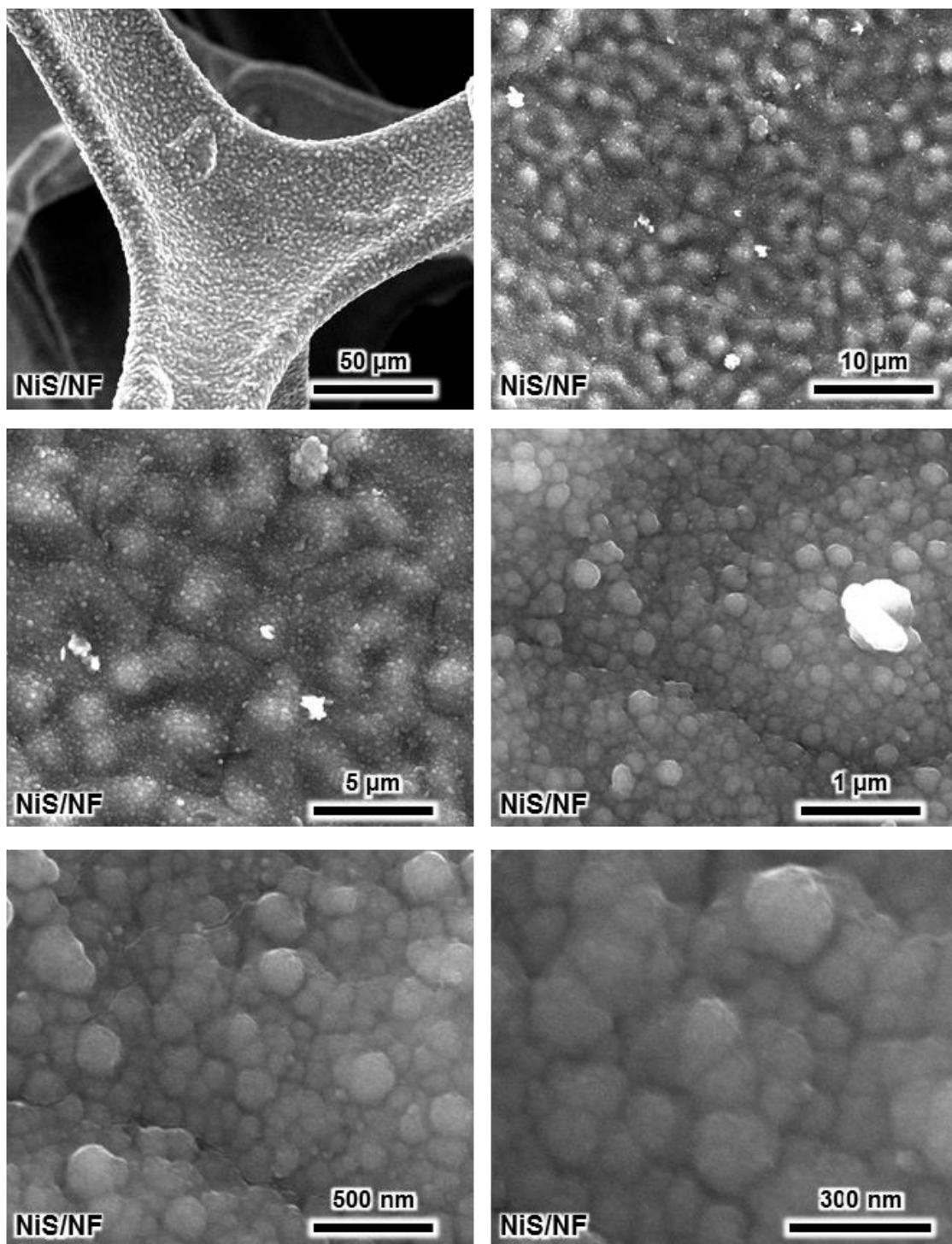


Figure S5. SEM images of the pristine NiS/NF electrode at different magnifications.

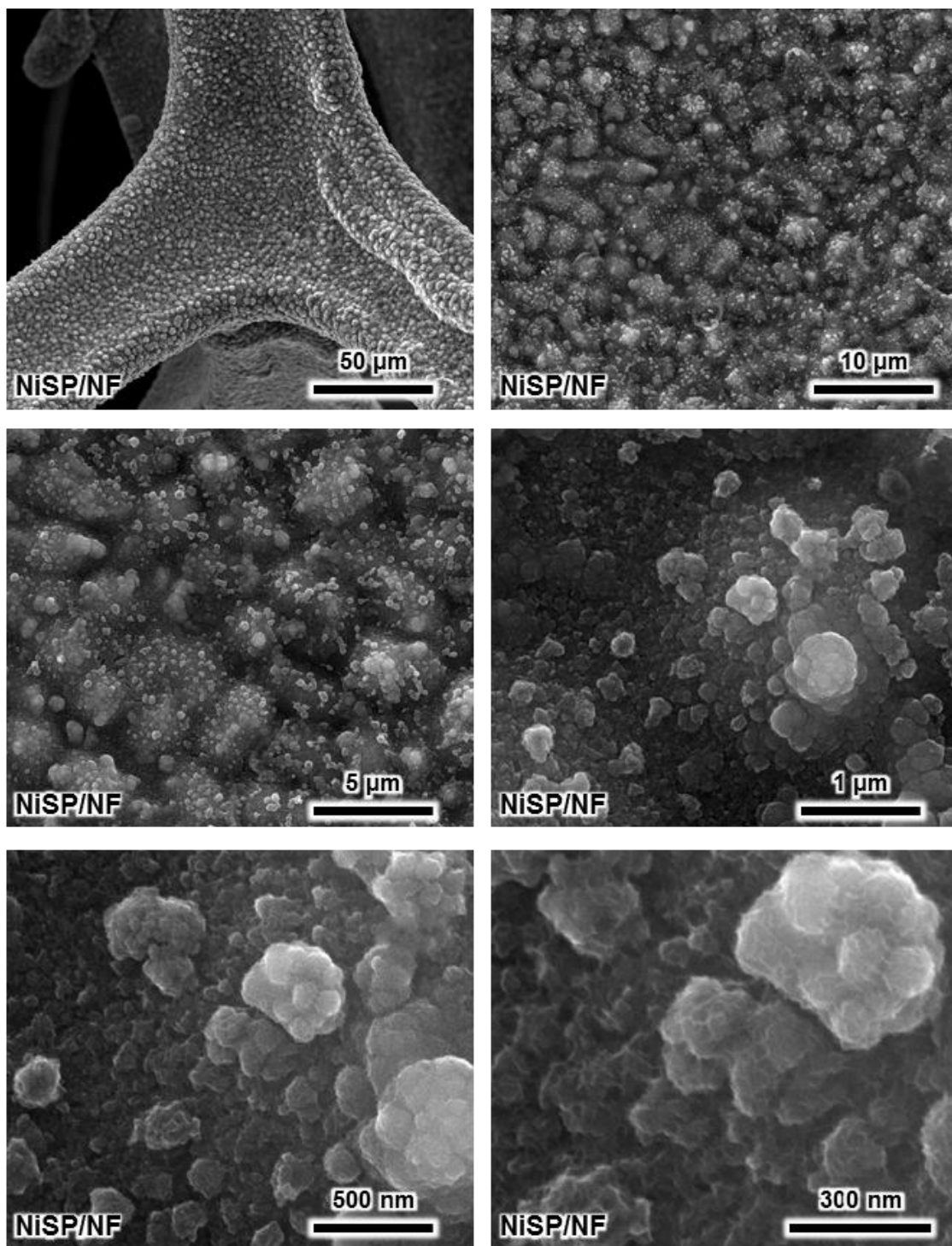


Figure S6. SEM images of the pristine NiSP/NF electrode at different magnifications.

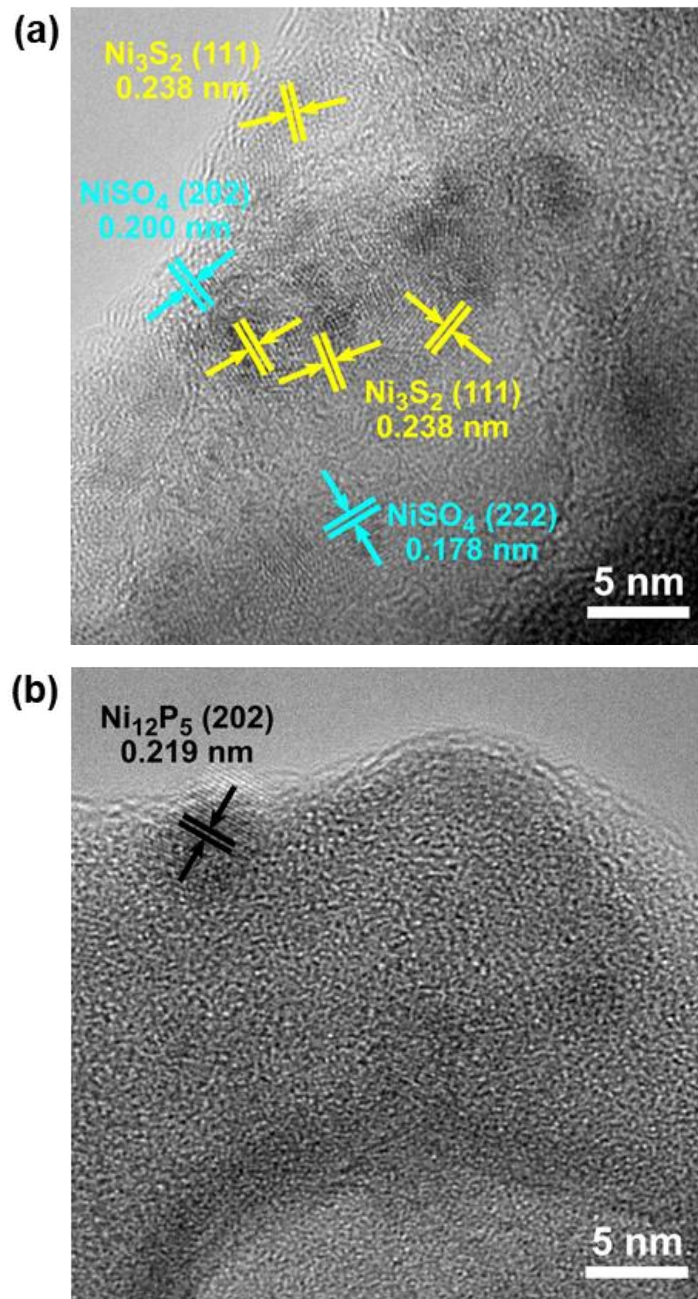


Figure S7. Additional high-resolution TEM images of (a) NiS/NF and (b) NiP/NF samples.

Table S1. Comparison of the OER performance in alkaline media (1 M KOH) of different S-P electrocatalytic films prepared by electrodeposition.

Material	Substrate	Mass loading (mg cm⁻²)	η_{10} (mV)	η_{50} (mV)	η_{100} (mV)	Tafel slope (mV dec⁻¹)	Ref.
NiCoP-NiCoSe ₂	Carbon cloth	0.073	243	~270	~290	52	1
NiCoP	Carbon cloth	-	275	~315	~330	87	1
Ni-P	Ni foam	-	~255	~330	386	88	2
Ni-S	Ni foam	-	-	~325	370	87	2
Ni-S-P	Ni foam	-	219	~320	358	82	2
CoP-MNA	Ni foam	6.2	290	~330	~365	65	3
Ni _{0.51} Co _{0.49} P	Ni foam	-	239	~290	~300	45	4
NiP	Ni foam	-	362	~430	~460	112	4
CoP	Ni foam	-	329	~370	~390	77	4
Ni-P	Carbon fiber	14.2	~150	~310	-	73	5
Ni-Fe-Co-S	Cu foil	-	207	~260	272	63	6
Ni-Fe-S	Cu foil	-	225	~280	292	43	6
Ni-Co-S	Cu foil	-	266	~320	360	92	6
Ni-S	Cu foil	-	289	~400	419	115	6
Co-S	Ti mesh	-	361	~400	~430	64	7
CoS-A	Carbon cloth	~1.6	390	~480	~570	-	8
CoNiP	Ni foam	-	~310	~340	~390	~93	9
NiP _x	Carbon fiber	~4.3	200	~320	~430	55	10
Co~70P~30	Cu foil	-	358	~420	-	-	11
NiS	Ni foam	~3.1	294	453	575	168	This work
NiP	Ni foam	~2.5	325	501	695	108	This work
NiSP	Ni foam	~4.8	259	341	395	99	This work

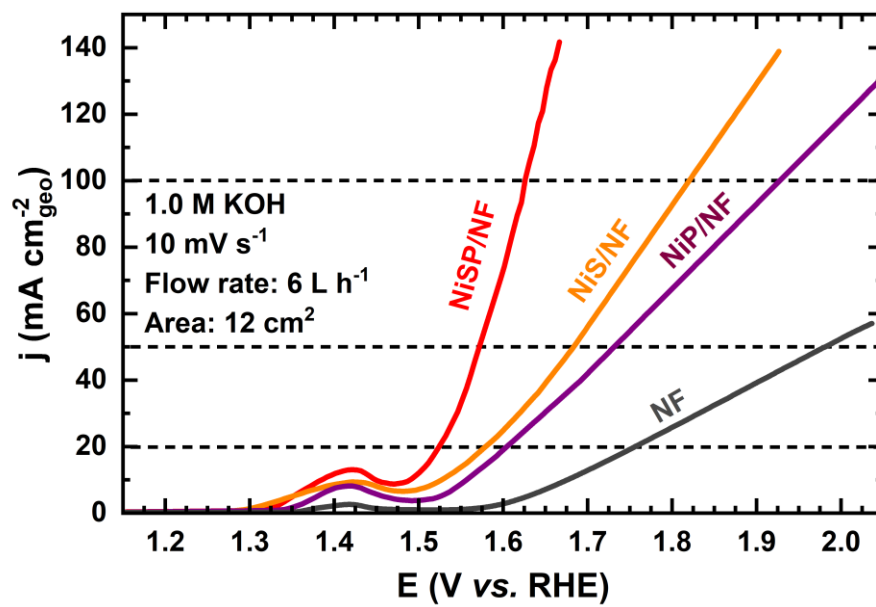


Figure S8. OER polarization curves of the as-prepared electrocatalytic films at higher current densities.

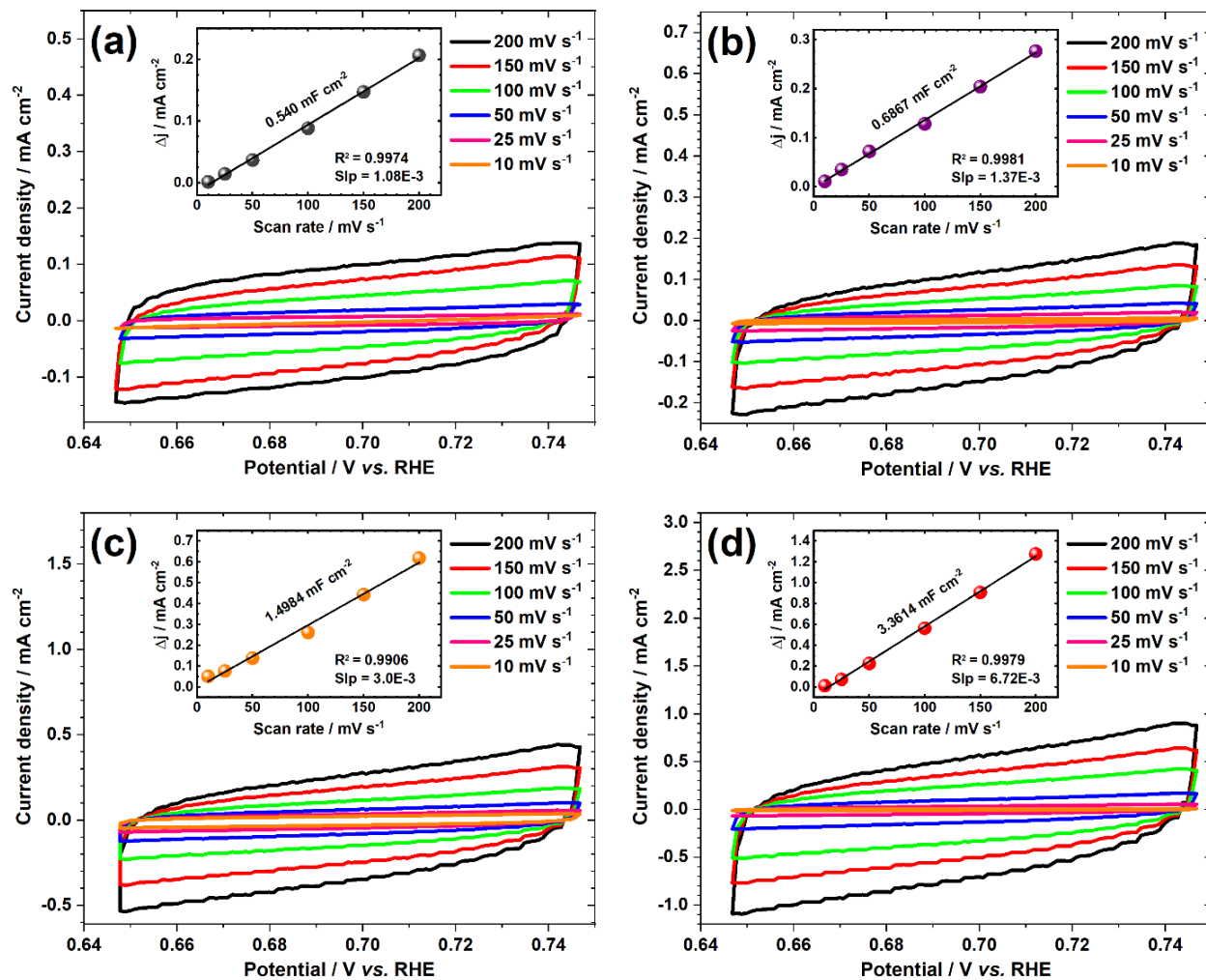


Figure S9. ECSA estimation of the as-prepared electrodes: (a) bare NF, (b) NiP/NF, (c) NiS/NF, and (d) NiSP/NF.

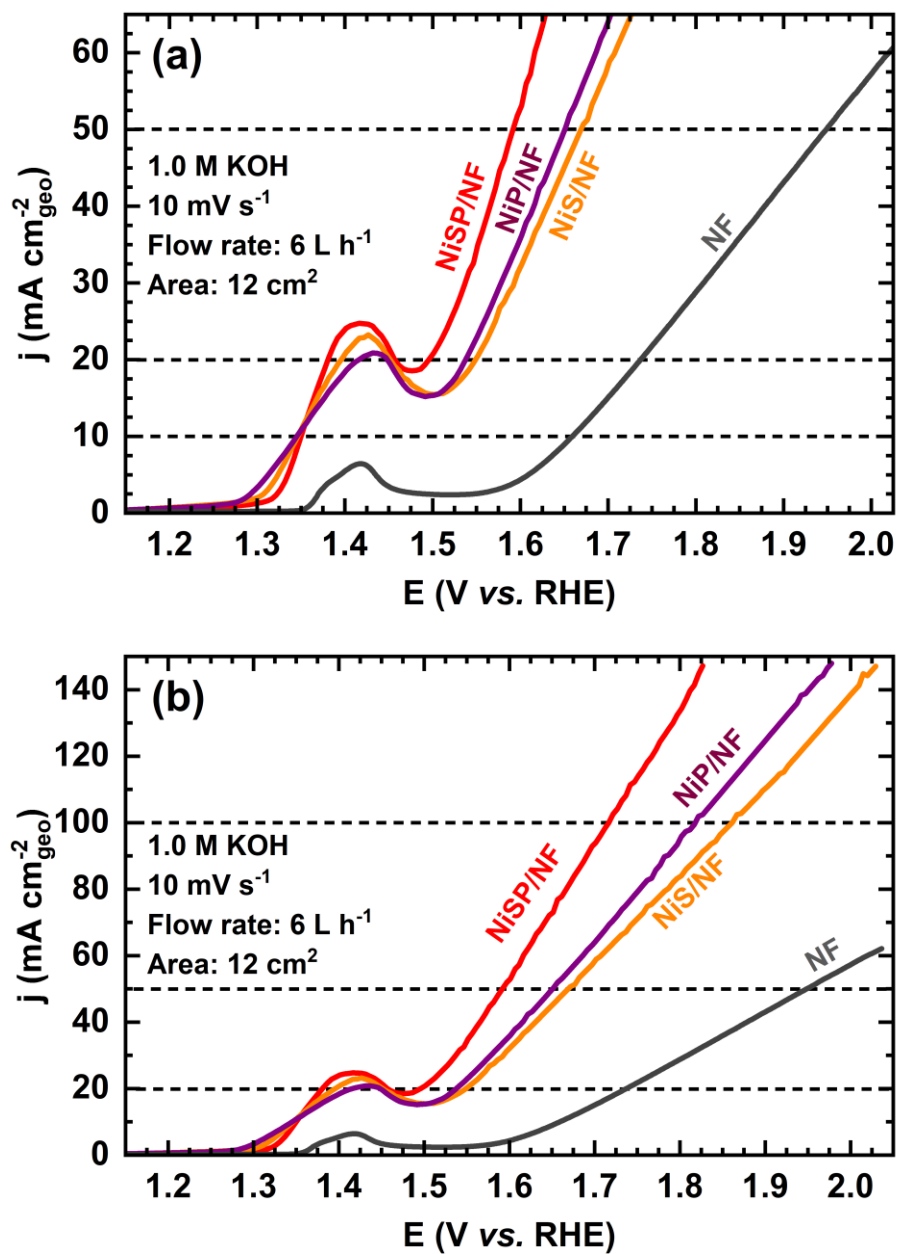


Figure S10. OER polarization curves of the evaluated electrocatalytic films after 20 h chronopotentiometric tests at 20 mA·cm⁻²: (a) close-up for low current densities and (b) high current densities.

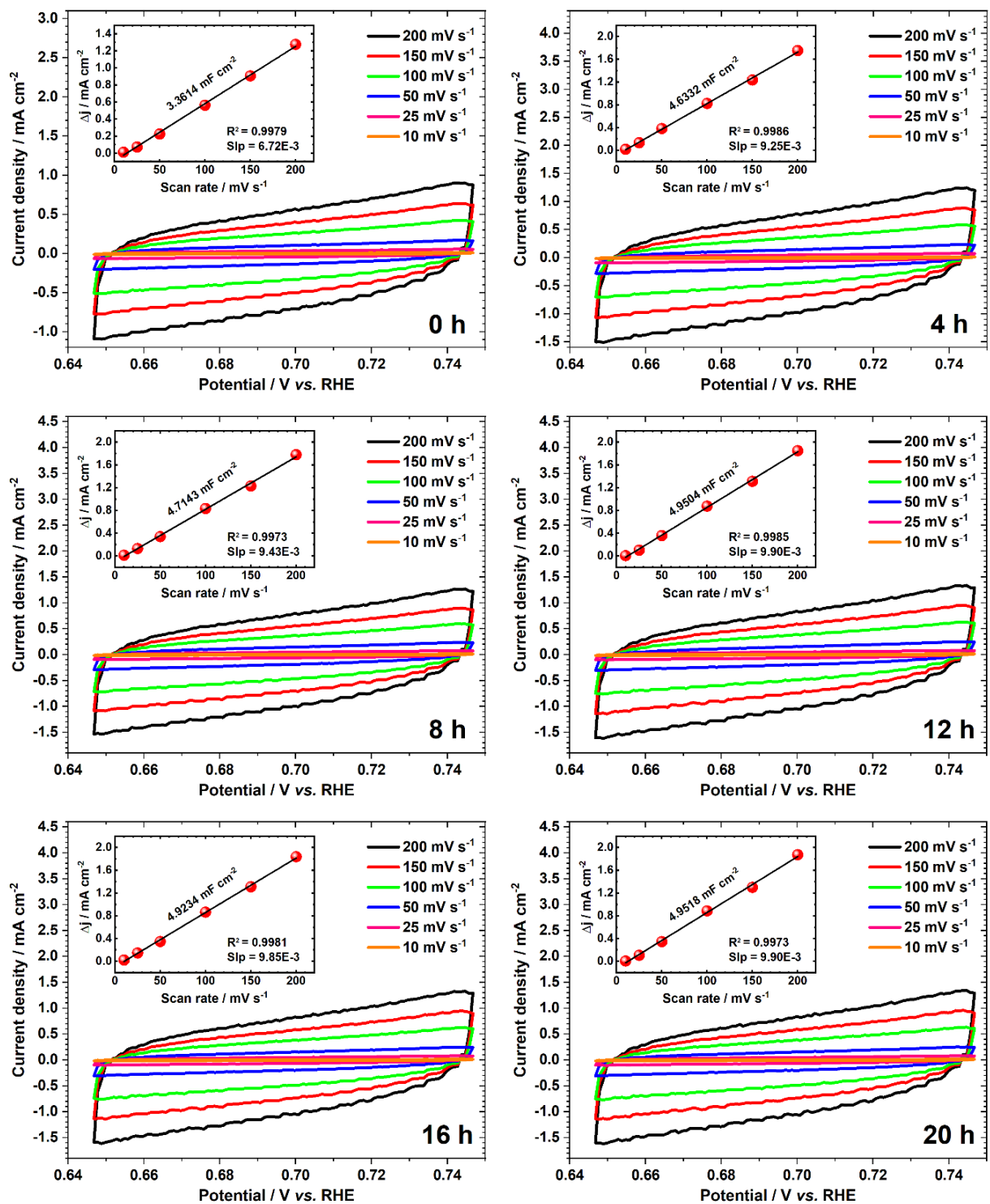


Figure S11. CV scans used to monitor the ECSA of the NiSP/NF electrode during OER stability tests.

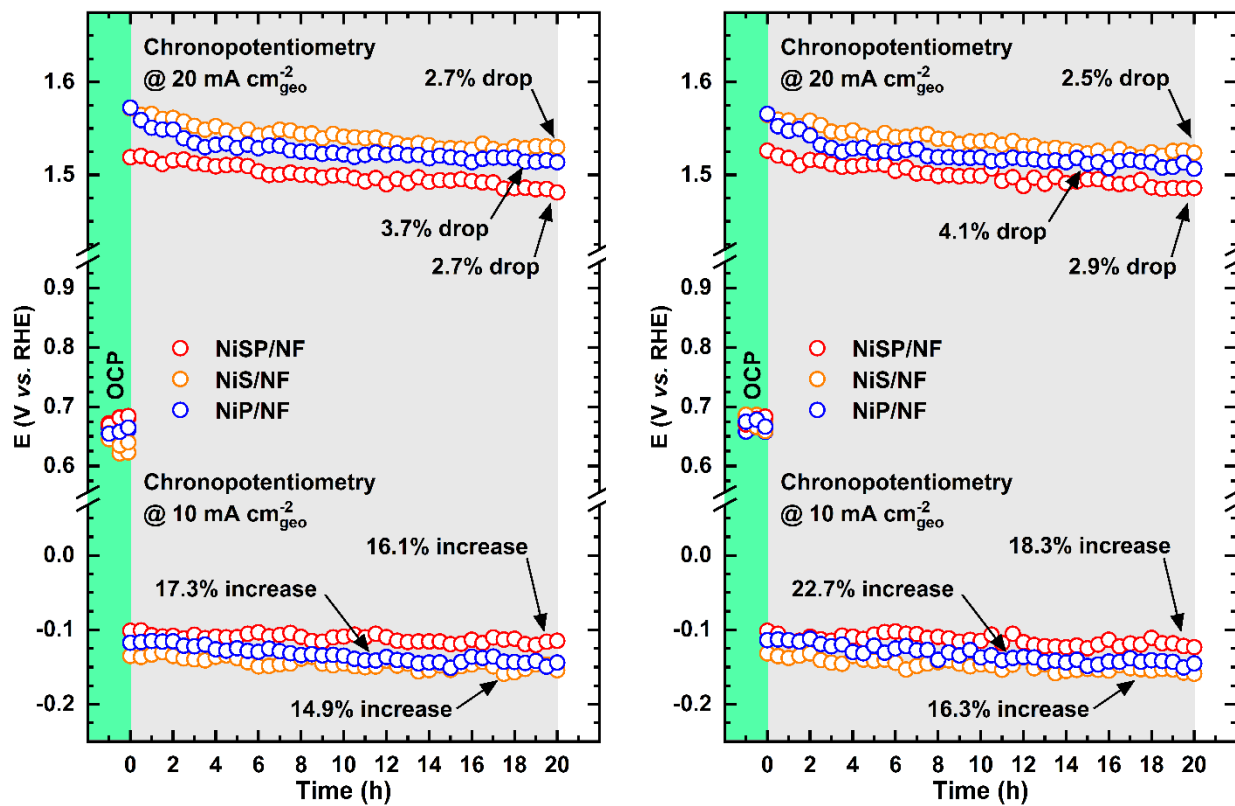


Figure S12. Chronopotentiometric replicates at $20 \text{ mA} \cdot \text{cm}^{-2}$ during a period of 20 h in 1 M KOH electrolyte for both the OER (positive potentials) and the HER (negative potentials).

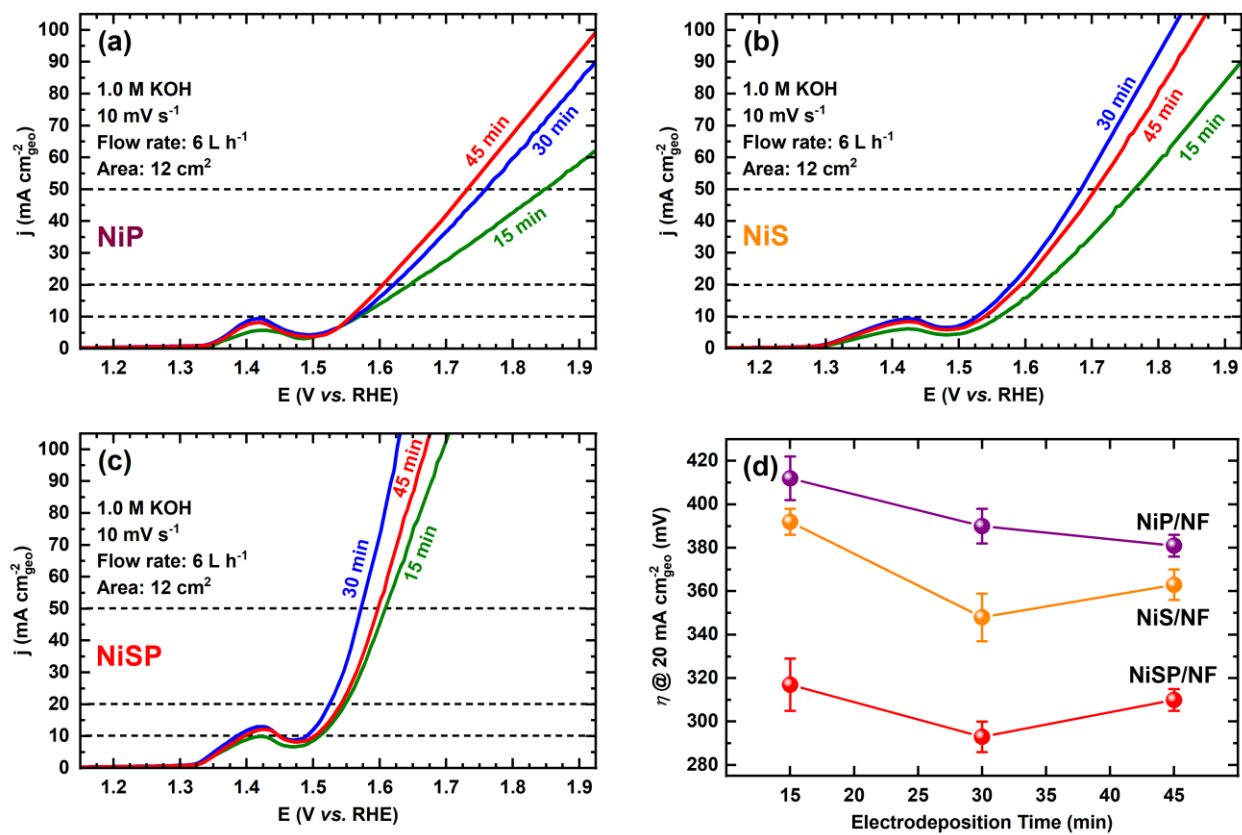


Figure S13. Electrodeposition optimization analysis at different deposition times for (a) NiP, (b) NiS and (c) NiSP films. (d) Comparison plot of the observed activity trends at 20 mA·cm⁻².

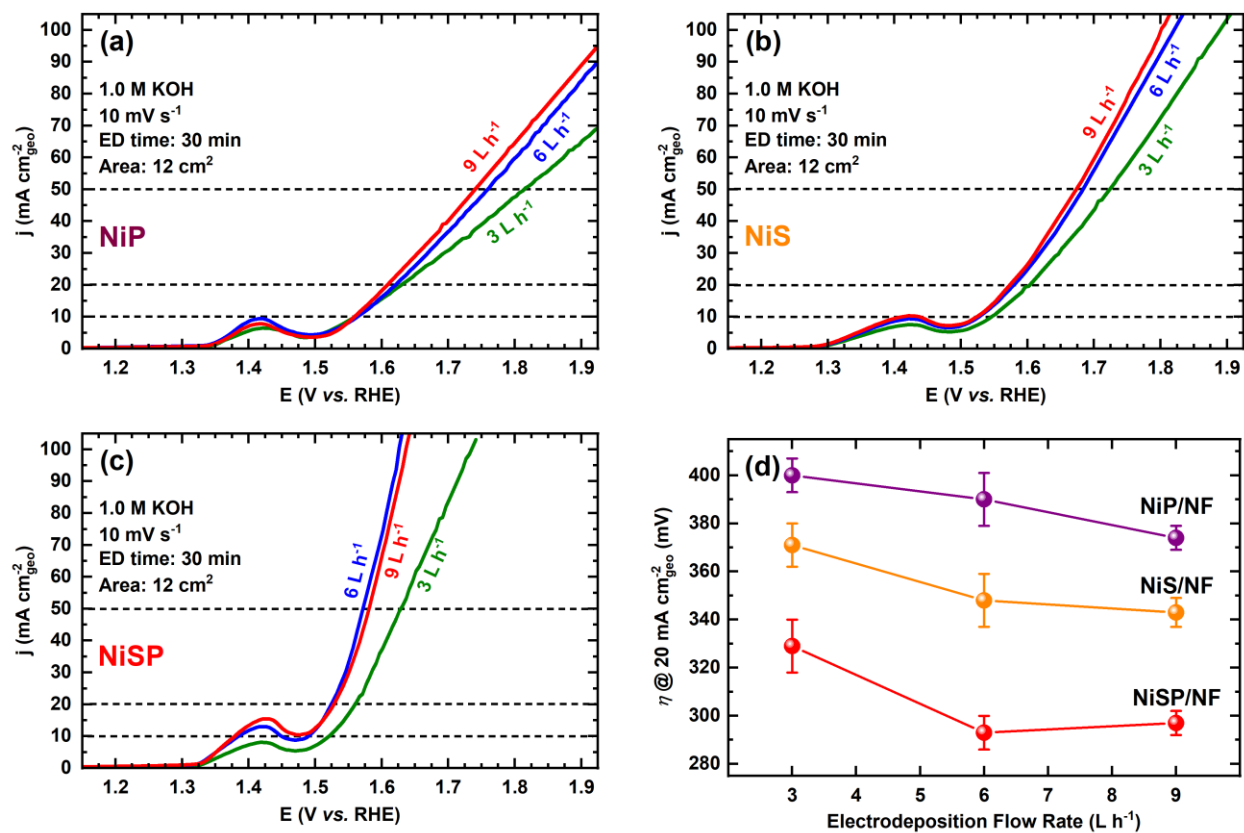


Figure S14. Electrodeposition optimization analysis at different volumetric flow rates for (a) NiP, (b) NiS and (c) NiSP films. (d) Comparison plot of the observed activity trends at 20 mA·cm⁻².

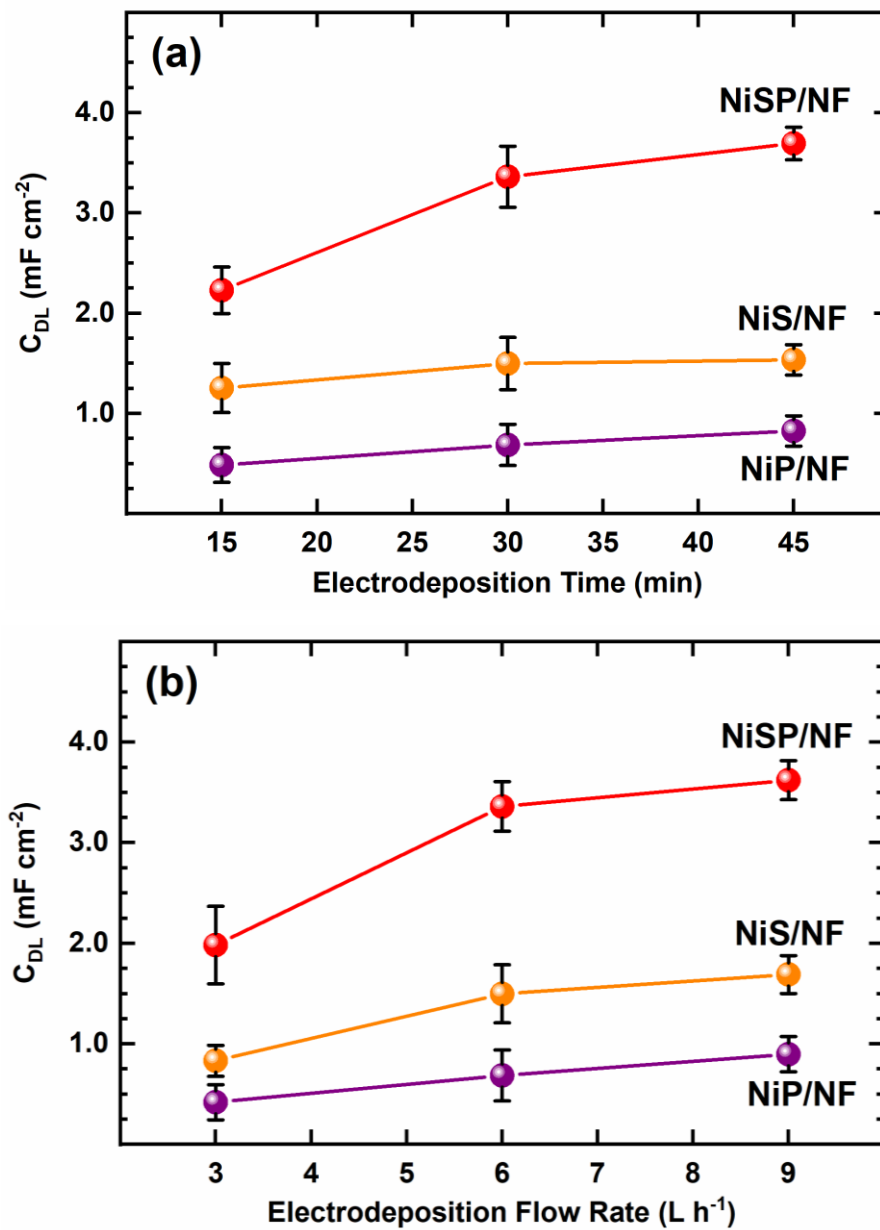


Figure S15. Comparison plot of the observed ECSA trends during electrodeposition optimization analysis when varying (a) deposition times and (b) volumetric flow rates. Significant changes were only seen in the NiSP/NF film.

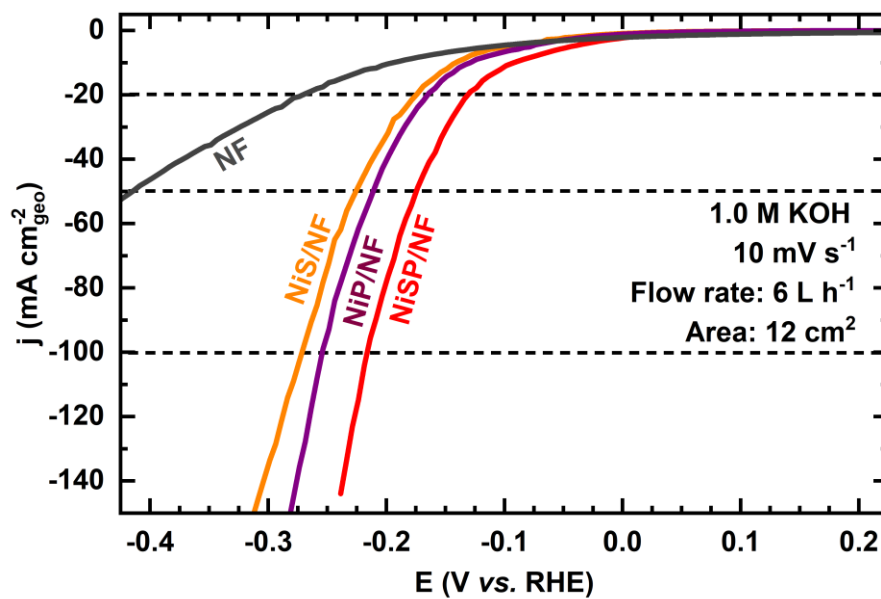


Figure S16. HER polarization curves of the as-prepared electrocatalytic films at higher current densities.

Table S2. Comparison of the HER performance in alkaline media (1 M KOH) of different S-P electrocatalytic films prepared by electrodeposition.

Material	Substrate	Mass loading (mg cm⁻²)	η_{10} (mV)	η_{50} (mV)	η_{100} (mV)	Tafel slope (mV dec⁻¹)	Ref.
CoNiP	Ni foam	-	111	~180	~220	97	9
Ni-Fe-Co-S	Cu foil	-	106	~180	215	95	6
Ni-Fe-S	Cu foil	-	123	~200	235	116	6
Ni-Co-S	Cu foil	-	148	~240	281	113	6
Ni-S	Cu foil	-	174	~280	336	142	6
NiCoP	Carbon cloth	-	218	~375	~460	-	1
NiCoP-NiCoSe ₂	Carbon cloth	0.073	196	~300	~350	-	1
Ni _{0.51} Co _{0.49} P	Ni foam	-	82	~130	~145	43	4
NiP	Ni foam	-	~235	~325	~345	~135	4
CoP	Ni foam	-	~210	~260	~275	~77	4
CoP-MNA	Ni foam	6.2	54	~100	121	51	3
Ni-S-P	Ni foam	-	120	~170	194	71	2
Ni-P	Ni foam	-	134	~190	210	61	2
Ni-S	Ni foam	-	315	~410	430	109	2
NiP _x	Carbon fiber	~4.3	118	-	-	48	10
NiS	Ni foam	~3.1	143	225	271	115	This work
NiP	Ni foam	~2.5	129	210	253	114	This work
NiSP	Ni foam	~4.8	93	174	217	107	This work

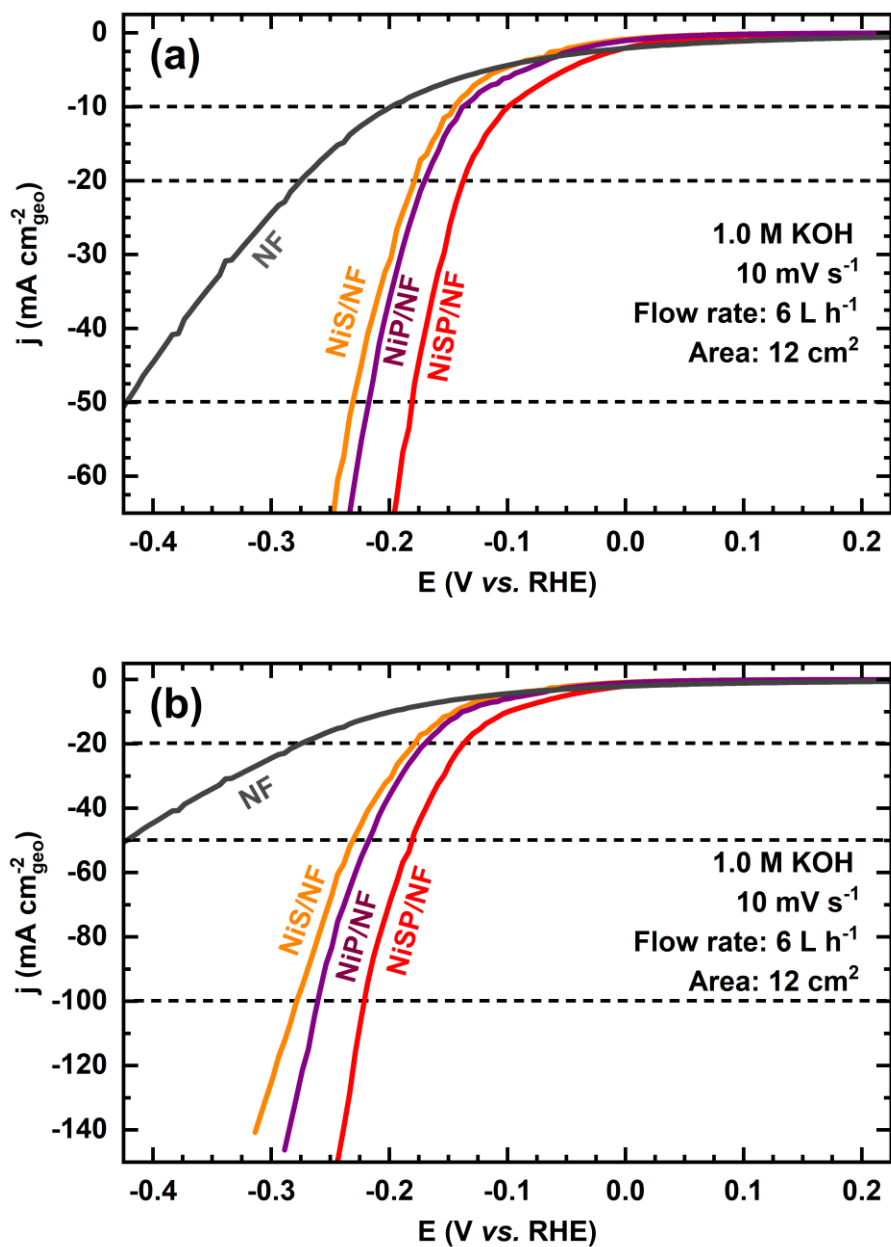


Figure S17. HER polarization curves of the evaluated electrocatalytic films after 20 h chronopotentiometric tests at $-20 \text{ mA}\cdot\text{cm}^{-2}$: (a) close-up for low current densities and (b) high current densities.

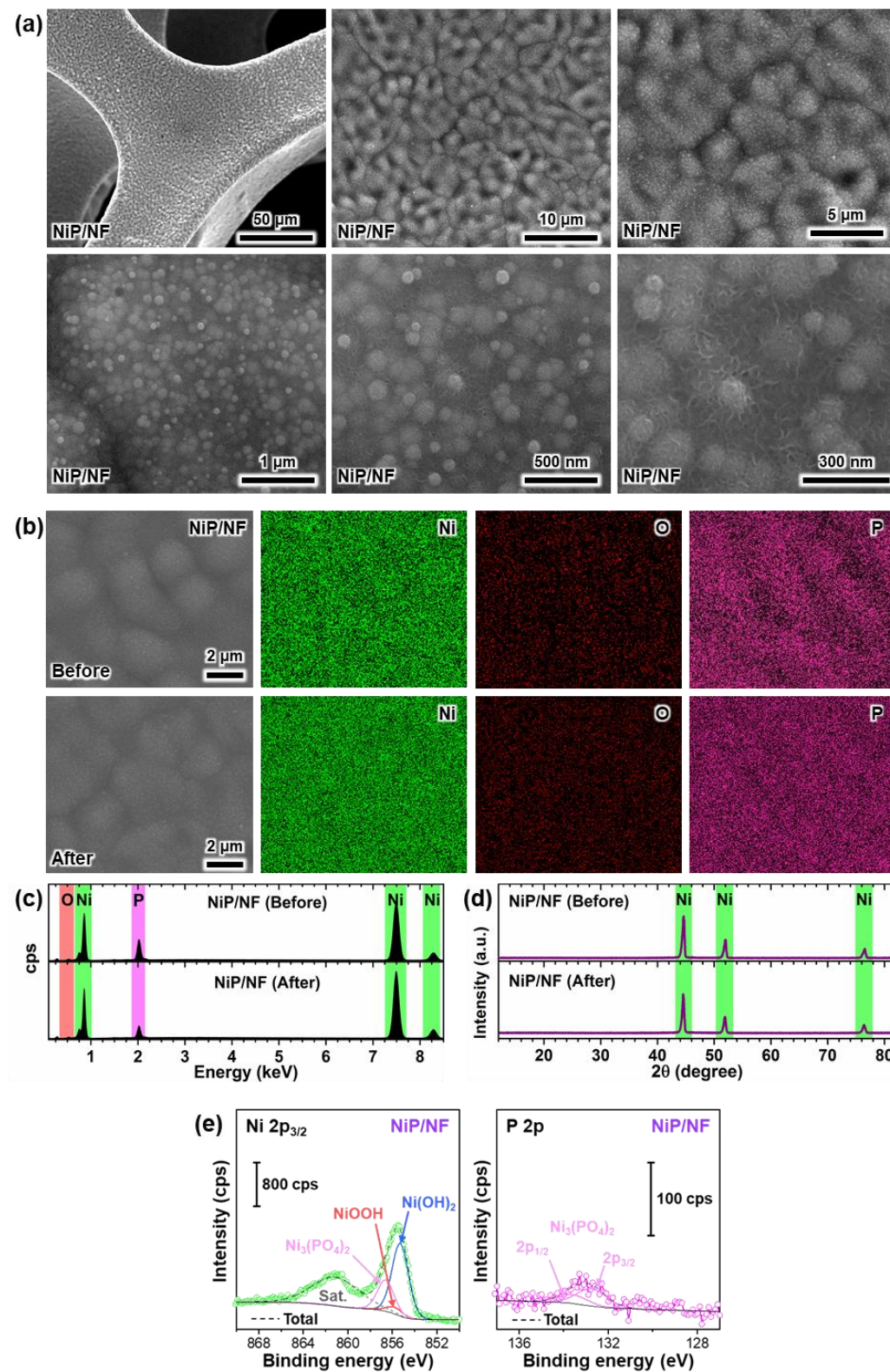


Figure S18. Post analysis of the NiP/NF electrode after the OER: (a) SEM images at different magnifications, (b) elemental mapping, (c) EDX spectra and (d) XRD comparison before and after OER tests, (e) XPS results.

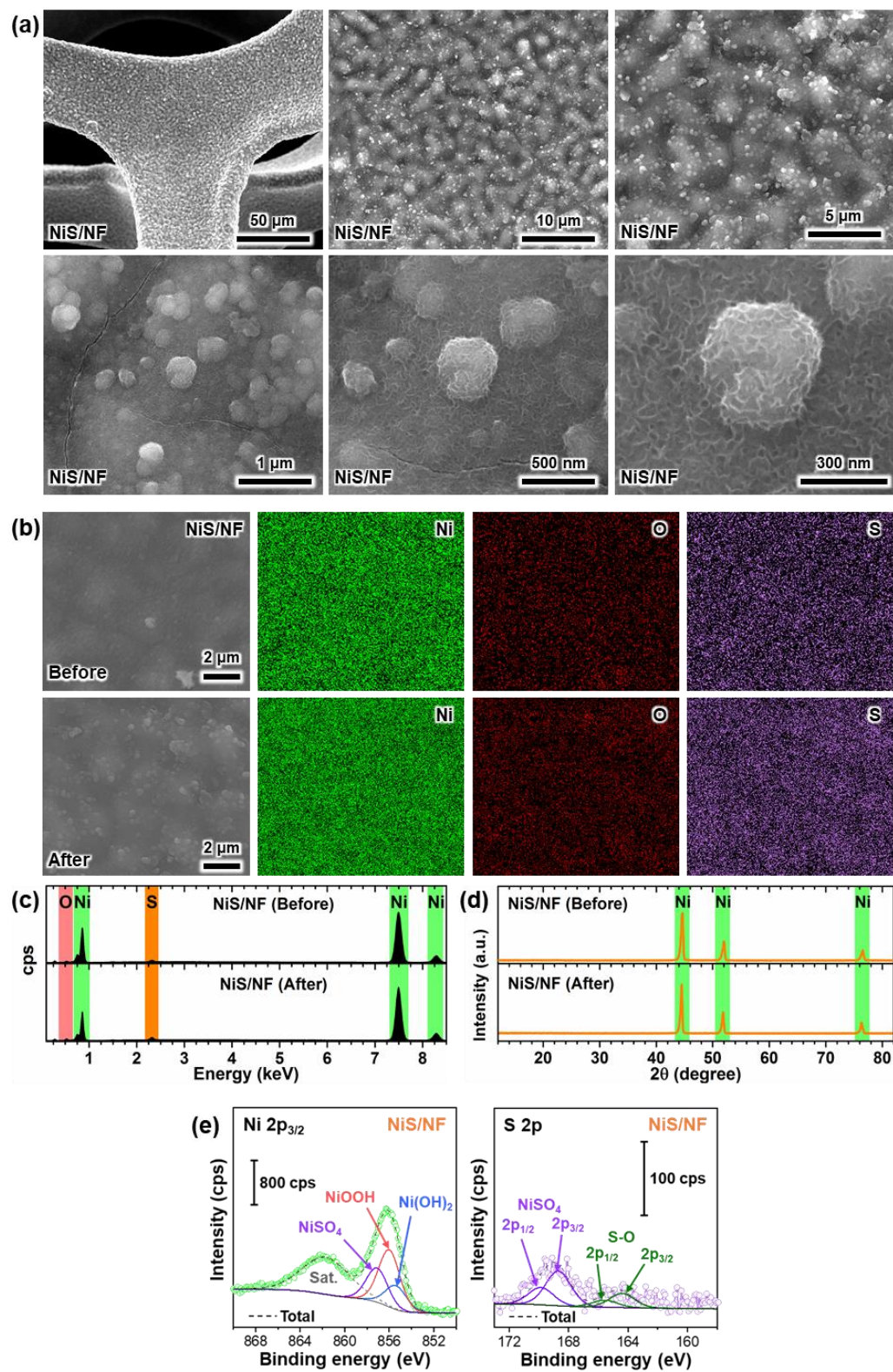


Figure S19. Post analysis of the NiS/NF electrode after the OER: (a) SEM images at different magnifications, (b) elemental mapping, (c) EDX spectra and (d) XRD comparison before and after OER tests, (e) XPS results.

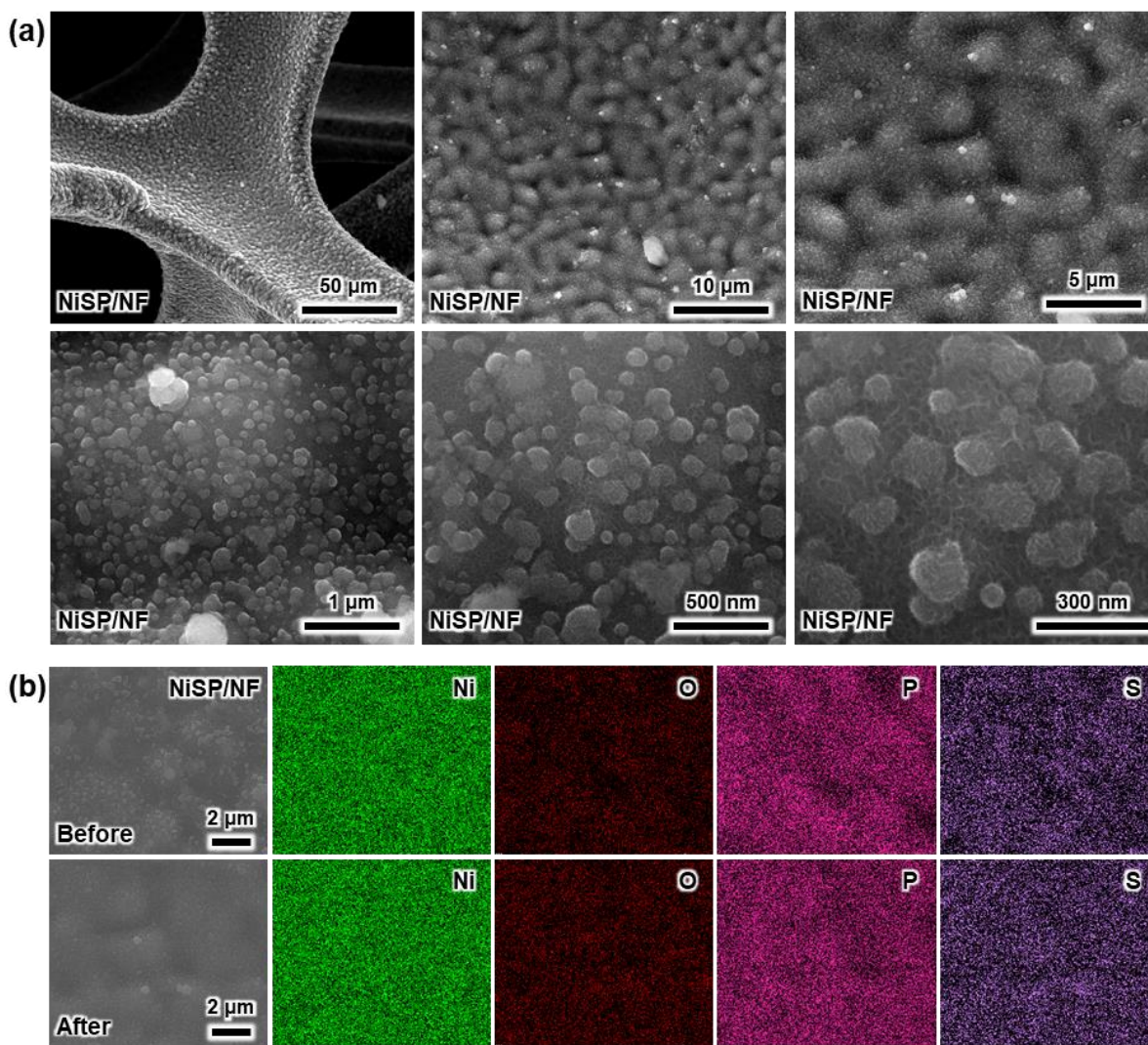


Figure S20. Post analysis of the NiSP/NF electrode after the OER: (a) SEM images at different magnifications, (b) elemental mapping before and after OER tests.

Table S3. Atomic composition (%) from EDX spectra before and after the OER.

Element	Before	After
NiP/NF		
Ni	48.81 ± 5.48	57.12 ± 5.91
O	4.68 ± 0.97	8.31 ± 0.69
P	14.65 ± 1.47	8.85 ± 0.86
NiS/NF		
Ni	59.67 ± 6.29	61.80 ± 6.30
O	5.12 ± 0.88	7.87 ± 1.25
S	1.20 ± 0.18	2.24 ± 0.48
NiSP/NF		
Ni	51.54 ± 5.68	49.25 ± 5.66
O	6.97 ± 1.10	8.91 ± 0.60
P	12.05 ± 1.21	9.29 ± 0.99
S	1.93 ± 0.25	1.79 ± 0.25

Table S4. Concentration (in ppm) of dissolved elements in the KOH electrolyte before and after stability experiments determined by TXRF measurements.

Element	Before OER	After OER	Before HER	After HER
NiP/NF				
Ni	0.318	0.431	0.254	0.370
Fe	Not det.	Not det.	Not det.	Not det.
P	Not det.	0.689	Not det.	0.992
NiS/NF				
Ni	0.402	0.716	0.521	0.444
Fe	Not det.	Not det.	Not det.	Not det.
S	Not det.	Not det.	Not det.	0.841
NiSP/NF				
Ni	0.360	0.560	0.483	0.441
Fe	Not det.	Not det.	Not det.	Not det.
P	Not det.	0.485	Not det.	0.892
S	Not det.	Not det.	Not det.	0.937
Limits of detection: Ni (0.022), P (0.330), S (0.800), Fe (0.024)				

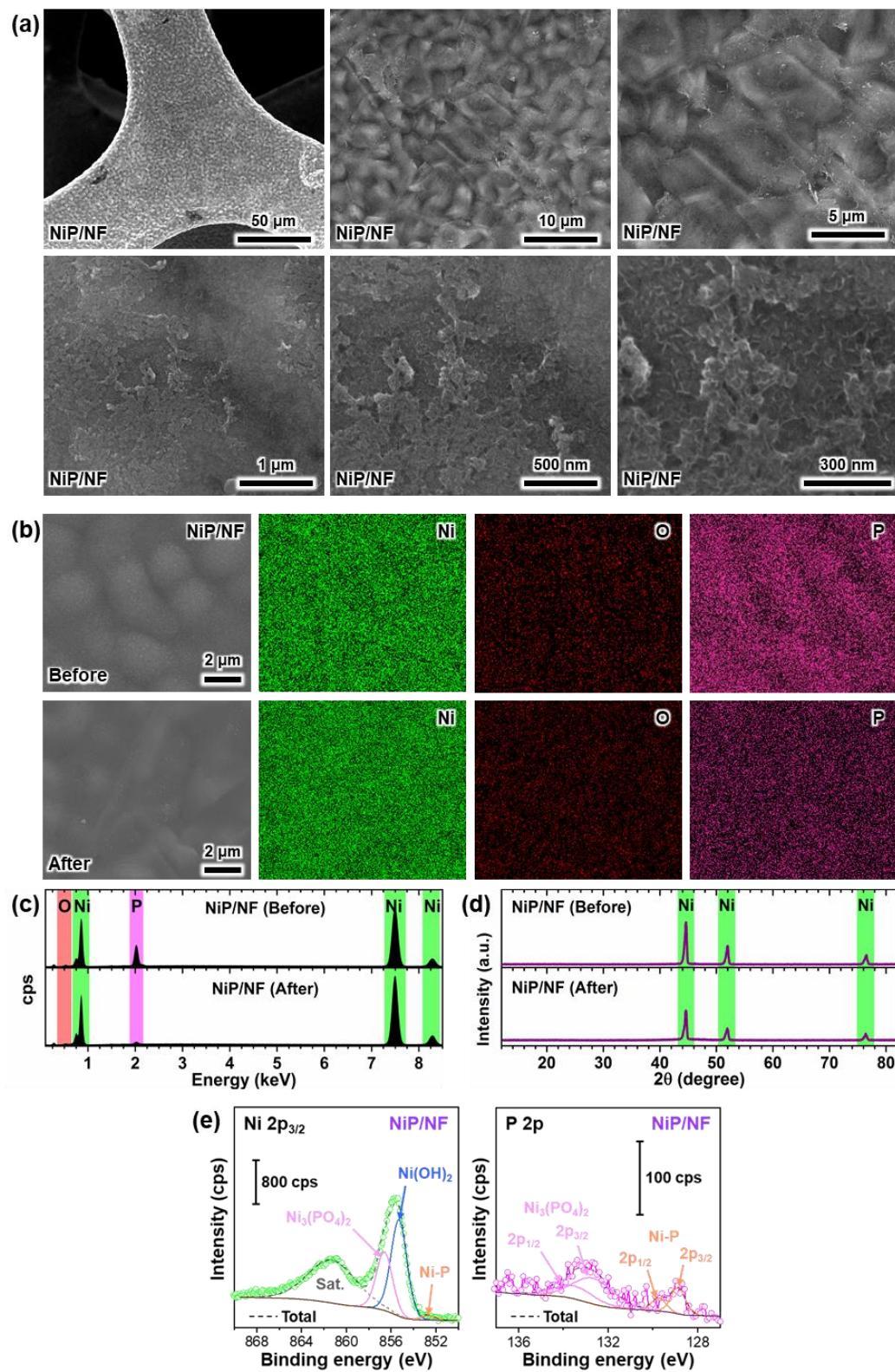


Figure S21. Post analysis of the NiP/NF electrode after HER: (a) SEM images at different magnifications, (b) elemental mapping, (c) EDX spectra and (d) XRD comparison before and after HER tests, (e) XPS results.

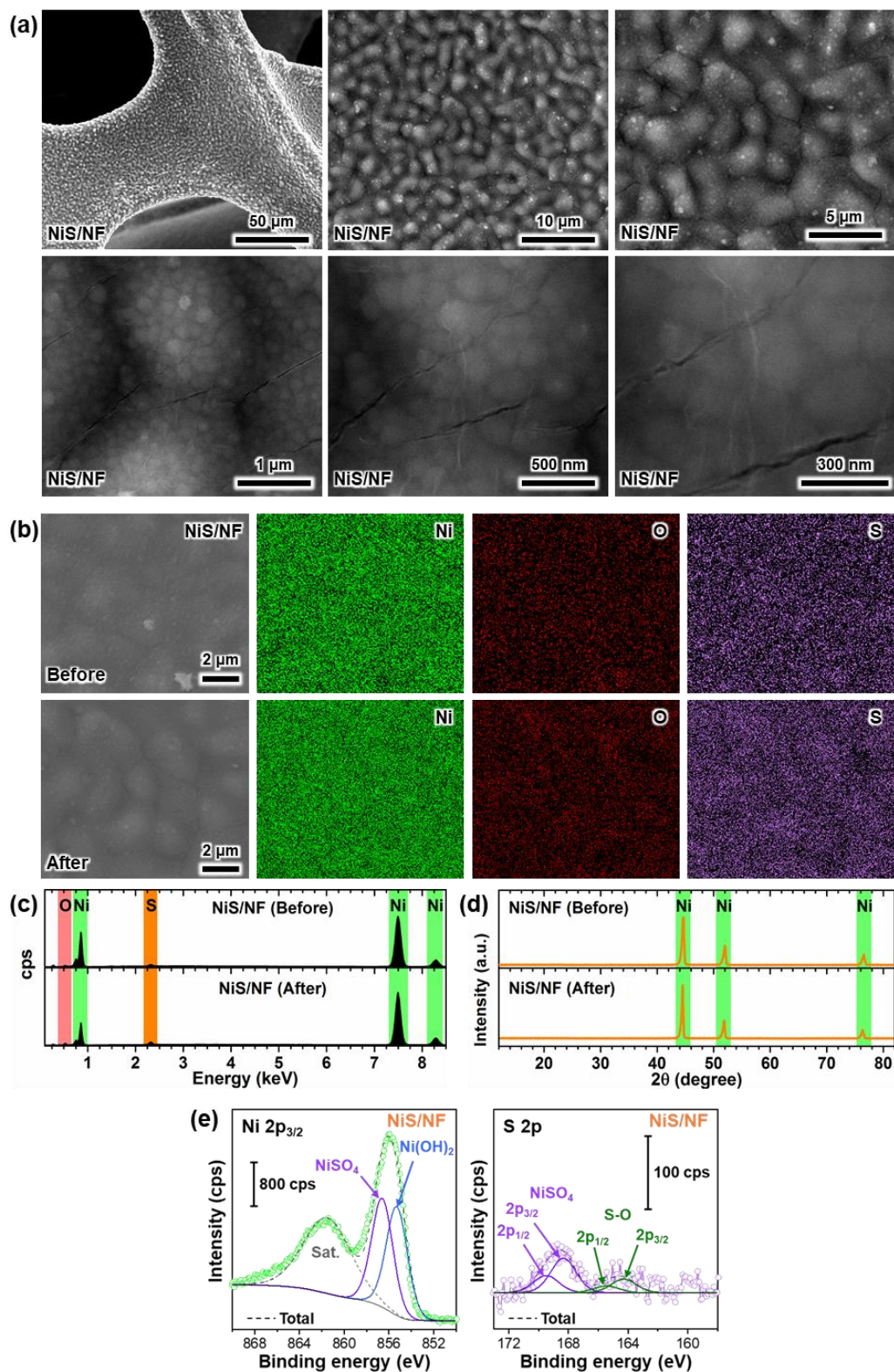


Figure S22. Post analysis of the NiS/NF electrode after HER: (a) SEM images at different magnifications, (b) elemental mapping, (c) EDX spectra and (d) XRD comparison before and after HER tests, (e) XPS results.

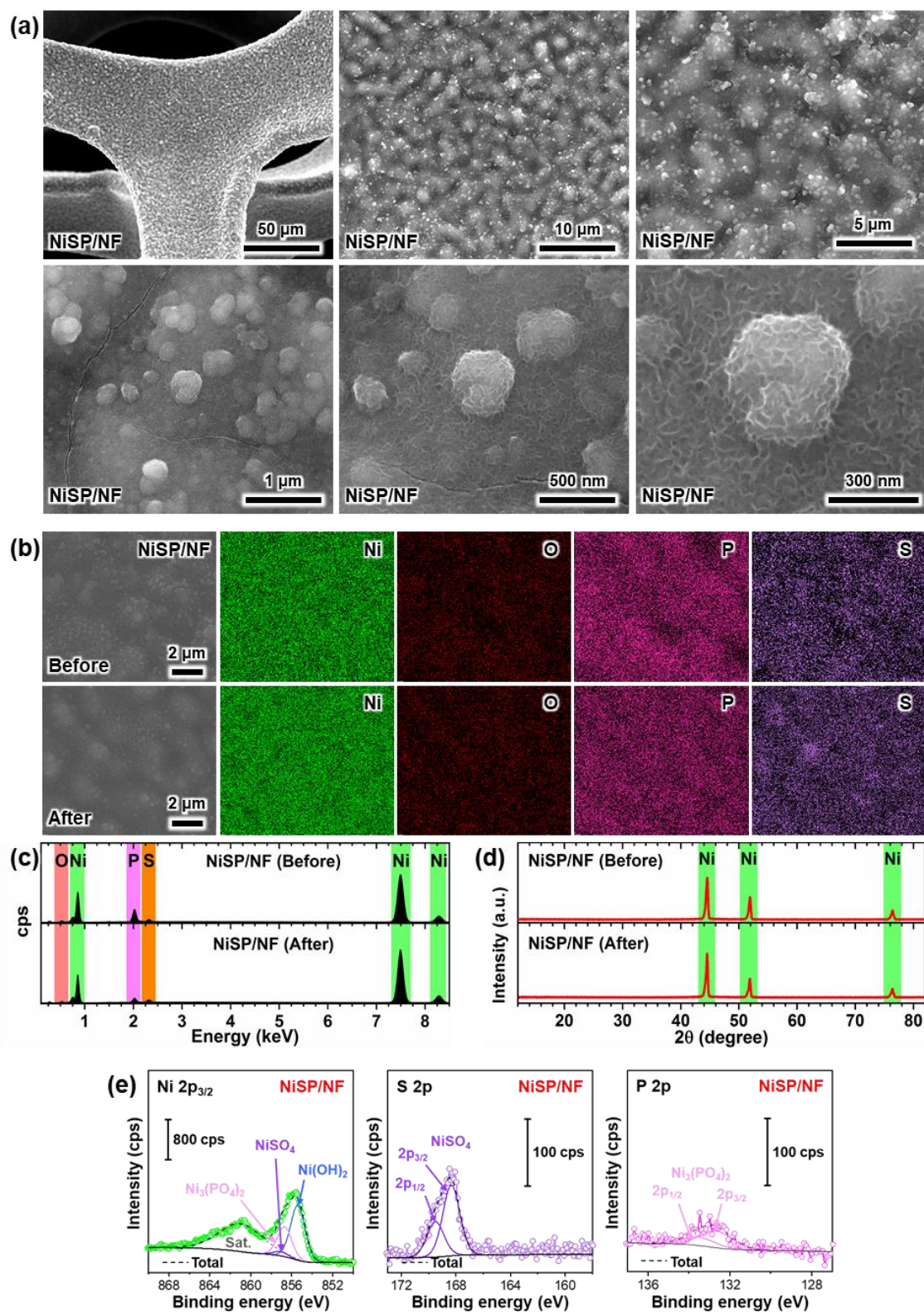


Figure S23. Post analysis of the NiSP/NF electrode after HER: (a) SEM images at different magnifications, (b) elemental mapping, (c) EDX spectra and (d) XRD comparison before and after HER tests, (e) XPS results.

Table S5. Atomic composition (%) from EDX spectra before and after HER.

Element	Before	After
NiP/NF		
Ni	48.81 ± 5.48	69.09 ± 8.21
O	4.68 ± 0.97	2.36 ± 0.71
P	14.65 ± 1.47	1.53 ± 0.24
NiS/NF		
Ni	59.67 ± 6.29	65.69 ± 6.66
O	5.12 ± 0.88	6.00 ± 1.48
S	1.20 ± 0.18	2.04 ± 0.53
NiSP/NF		
Ni	51.54 ± 5.68	61.99 ± 6.49
O	6.97 ± 1.07	4.19 ± 1.03
P	12.05 ± 1.21	4.59 ± 0.48
S	1.93 ± 0.25	2.25 ± 0.27

Table S6. Comparison of overall water splitting performance in alkaline media (1 M KOH) of different S-P electrocatalytic films prepared by electrodeposition.

Electrode couple	Substrate	Cell voltage (V @ 10 mA cm⁻²)	Cell voltage (V @ 100 mA cm⁻²)	Ref.
Ni-S-P Ni-S-P	Ni foam	1.58	~1.79	2
Ni-S Ni-S	Ni foam	1.75	~2.10	2
Ni-P Ni-P	Ni foam	1.63	~1.88	2
NiCoP–NiCoSe ₂	Carbon cloth	1.70	~2.07	1
Ni _{0.51} Co _{0.49} P	Ni foam	1.57	~1.70	4
NiP NiP	Ni foam	~1.69	~1.87	4
CoP CoP	Ni foam	~1.63	~1.77	4
CoNiP CoNiP	Ni foam	1.61	~1.95	9
CoP-MNA CoP-MNA	Ni foam	1.62	-	3
Ni-P Ni-P	Carbon fiber	1.63	2.50	5
NiP _x NiP _x	Carbon fiber	1.61	-	10
Ni-Fe-Co-S Ni-Fe-Co-S	Cu foil	1.54	-	6
Ni-Co-S Ni-Co-S	Cu foil	~1.62	-	6
Ni-Fe-S Ni-Fe-S	Cu foil	~1.56	-	6
Ni-S Ni-S	Cu foil	~1.70	-	6
NiSP NiSP	Ni foam	1.70	1.85	This work

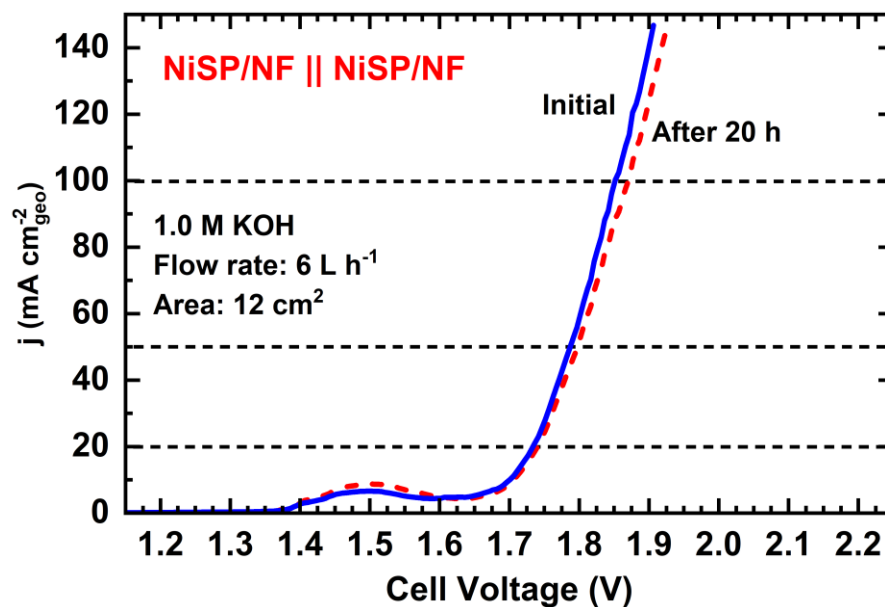


Figure S24. Overall water splitting polarization curves before and after galvanostatic runs at 10 mA·cm⁻² during a period of 20 h.

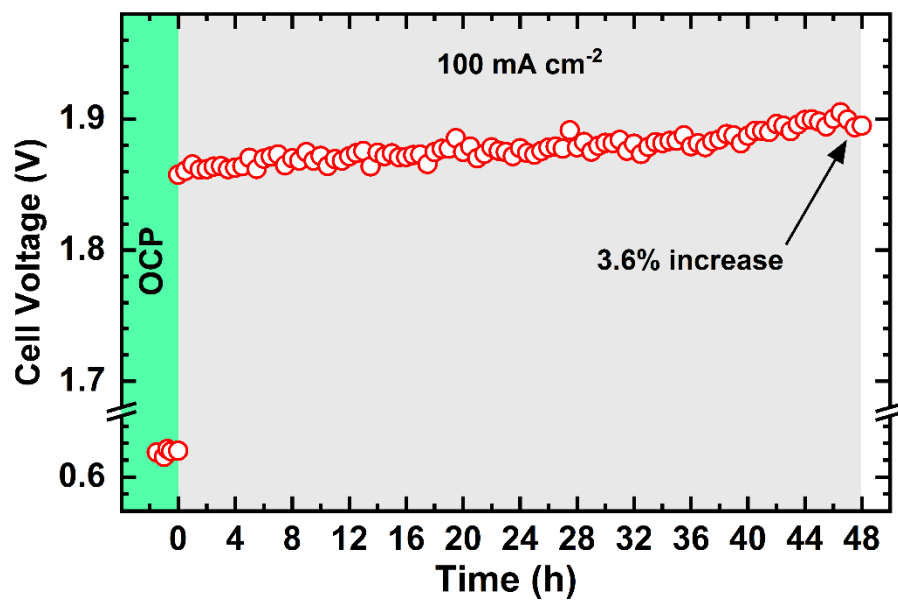


Figure S25. Long-term electrolysis test at 100 mA·cm⁻² during a period of 48 h. Note: the experiment was performed using a power supply to withstand the high current (1 A) for two days. Fluctuation is attributed to the intense bubbling at high current densities.

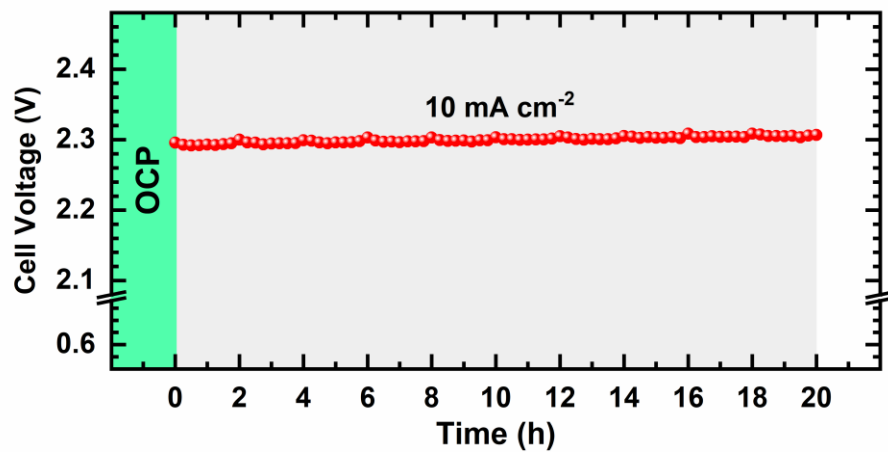


Figure S26. Chronopotentiometric run during gas evolution test at $10 \text{ mA} \cdot \text{cm}^{-2}$ during a period of 20 h.

References

- (1) Wang, T.; Liu, X.; Yan, Z.; Teng, Y.; Li, R.; Zhang, J.; Peng, T. Facile Preparation Process of NiCoP–NiCoSe₂ Nano-Bilayer Films for Oxygen Evolution Reaction with High Efficiency and Long Duration. *ACS Sustain. Chem. Eng.* **2020**, *8* (2), 1240–1251. <https://doi.org/10.1021/acssuschemeng.9b06514>.
- (2) Xu, Q.; Gao, W.; Wang, M.; Yuan, G.; Ren, X.; Zhao, R.; Zhao, S.; Wang, Q. Electrodeposition of NiS/Ni₂P Nanoparticles Embedded in Amorphous Ni(OH)₂ Nanosheets as an Efficient and Durable Dual-Functional Electrocatalyst for Overall Water Splitting. *Int. J. Hydrogen Energy* **2020**, *45* (4), 2546–2556. <https://doi.org/10.1016/j.ijhydene.2019.11.217>.
- (3) Zhu, Y.-P.; Liu, Y.-P.; Ren, T.-Z.; Yuan, Z.-Y. Self-Supported Cobalt Phosphide Mesoporous Nanorod Arrays: A Flexible and Bifunctional Electrode for Highly Active Electrocatalytic Water Reduction and Oxidation. *Adv. Funct. Mater.* **2015**, *25* (47), 7337–7347. <https://doi.org/10.1002/adfm.201503666>.
- (4) Yu, J.; Li, Q.; Li, Y.; Xu, C.-Y.; Zhen, L.; Dravid, V. P.; Wu, J. Ternary Metal Phosphide with Triple-Layered Structure as a Low-Cost and Efficient Electrocatalyst for Bifunctional Water Splitting. *Adv. Funct. Mater.* **2016**, *26* (42), 7644–7651. <https://doi.org/10.1002/adfm.201603727>.
- (5) Wang, X.; Li, W.; Xiong, D.; Petrovykh, D. Y.; Liu, L. Bifunctional Nickel Phosphide Nanocatalysts Supported on Carbon Fiber Paper for Highly Efficient and Stable Overall Water Splitting. *Adv. Funct. Mater.* **2016**, *26* (23), 4067–4077. <https://doi.org/10.1002/adfm.201505509>.
- (6) Darband, G. B.; Aliofkhazraei, M.; Hyun, S.; Rouhaghdam, A. S.; Shanmugam, S. Electrodeposition of Ni–Co–Fe Mixed Sulfide Ultrathin Nanosheets on Ni Nanocones: A Low-Cost, Durable and High Performance Catalyst for Electrochemical Water Splitting. *Nanoscale* **2019**, *11* (35), 16621–16634. <https://doi.org/10.1039/C9NR04529E>.
- (7) Liu, T.; Liang, Y.; Liu, Q.; Sun, X.; He, Y.; Asiri, A. M. Electrodeposition of Cobalt-Sulfide Nanosheets Film as an Efficient Electrocatalyst for Oxygen Evolution Reaction. *Electrochem. Commun.* **2015**, *60*, 92–96. <https://doi.org/10.1016/j.elecom.2015.08.011>.
- (8) Liu, B.; Qu, S.; Kou, Y.; Liu, Z.; Chen, X.; Wu, Y.; Han, X.; Deng, Y.; Hu, W.; Zhong, C. In Situ Electrodeposition of Cobalt Sulfide Nanosheet Arrays on Carbon Cloth as a Highly Efficient Bifunctional Electrocatalyst for Oxygen Evolution and Reduction Reactions. *ACS Appl. Mater. Interfaces* **2018**, *10* (36), 30433–30440. <https://doi.org/10.1021/acsaami.8b10645>.
- (9) Zhou, L.; Jiang, S.; Liu, Y.; Shao, M.; Wei, M.; Duan, X. Ultrathin CoNiP@Layered Double Hydroxides Core–Shell Nanosheets Arrays for Largely Enhanced Overall Water Splitting. *ACS Appl. Energy Mater.* **2018**, *1* (2), 623–631. <https://doi.org/10.1021/acsaem.7b00151>.
- (10) Zhang, Z.; Liu, S.; Xiao, J.; Wang, S. Fiber-Based Multifunctional Nickel Phosphide Electrodes for Flexible Energy Conversion and Storage. *J. Mater. Chem. A* **2016**, *4* (24), 9691–9699. <https://doi.org/10.1039/C6TA03732A>.
- (11) Chiu, C.-W.; Sun, I.-W.; Chen, P.-Y. Electrodeposition and Characterization of CoP Compounds Produced from the Hydrophilic Room-Temperature Ionic Liquid 1-Butyl-1-Methylpyrrolidinium Dicyanamide. *J. Electrochem. Soc.* **2017**, *164* (8), H5018. <https://doi.org/10.1149/2.0041708jes>.